Korean J. Chem. Eng., **30**(11), 2030-2036 (2013)
DOI: 10.1007/s11814-013-0150-4

Silver nanoparticles containing hybrid polymer microgels with tunable surface plasmon resonance and catalytic activity

Muhammad Ajmal*, Zahoor Hussain Farooqi, and Mohammad Siddiq*,†**

*Department of Chemistry, Quaid-I-Azam University, Islamabad 45320, Pakistan
**Institute of Chemistry, University of the Punjab, New Campus Lahore 54590, Pakistan
(*Received 16 May 2013 • accepted 5 August 2013*)

Abstract−Multi-responsive poly(N-isoprpylacrlamide-methacrylic acid-acrylamide) [P(NIPAM-MAA-AAm)] copolymer microgel was prepared by free radical emulsion polymerization. Silver nanoparticles were fabricated inside the microgel network by *in-situ* reduction of silver nitrate. Swelling and deswelling behavior of the pure microgels was studied under various conditions of pH and temperature using dynamic light scattering. A red shift was observed in surface plasmon resonance wavelength of Ag nanoparticles with pH induced swelling of hybrid microgel. The catalytic activity of the hybrid system was investigated by monitoring the reduction of p-nitrophenol under different conditions of temperature and amount of catalysts. For this catalytic reaction a time delay of 8 to 10 min was observed at room temperature, which was reduced to 2 min at high temperature due to swelling of microgels, which facilitated diffusion of reactants to catalyst surface and increased rate of reaction.

Key words: Microgels, Nanoparticles, Swelling, Catalysis, p-Nitrophenol

INTRODUCTION

Environmental degradation is affecting living and non-living components of the ecosystem. Industrial effluents, waste products and improper dumping of non-required materials cause this degradation. Aromatic nitrogenous compounds (like nitrophenols and nitrobenzene) are among the chief harmful pollutants present in industrial waste water [1]. p-Nitrophenol (4-NP) and similar derivatives are liberated from important industrial processes, such as from synthesis of pesticides, herbicides, insecticides and dyes [2]. This widespread occurrence of 4-NP motivated to proceed its breaking into p-aminophenol (4-AP) by nanoparticles. This is because 4-AP is less poisonous than 4-NP and there is great demand of 4-AP in many industries [3]. Moreover, nanoparticles effectively, rapidly and easily convert harmful 4-NP into 4-AP due to high surface to volume ratio of nanoparticles. Therefore, this reaction is very important for environmental, academic and technological purposes.

Nanoparticles are key subjects of recent research not only in the field of catalysis [4] but also for optical devices, [5] biosensors [6] and chemical separation [7] due to their tunable surface properties, but nanoparticles coagulate in aqueous medium. This aggregation limits their applications. Thus, the aggregation tendency of nanoparticles diminishes their use as catalyst. Stabilizing agents such as micelles, [8] dendrimers, [9] and microgels [10] have been used to increase the stability of nanoparticles. Many scientists have fabricated silver (Ag) and gold (Au) nanoparticles within temperature-sensitive microgels to make hybrid systems possessing tunable catalytic properties [11]. These hybrid systems are widely used as catalyst in aqueous medium because the reactants can easily diffuse into the network of microgels and can interact with metal nanoparticles entrapped inside this microgel network. Moreover, when the reaction is completed, hybrid microgels can easily be recycled by centrifugation. These advantages of hybrid microgels as catalysts have drawn considerable attention from the scientists working in catalysis presently [2,9,10,12-19]. In this context Zhang et al. employed polymer microgels as microreactors for the synthesis of nanoparticles inside the microgel network. They synthesized Ag, cadmium sulfide (CdS) and iron oxide (Fe_3O_4) nanoparticles, and reported that these hybrid microgels can be applied in catalysis, biolabeling, fabrication of polymer-based materials for photonic applications and chemical and biological separations [12]. Wunder et al. synthesized microgels functionalized with silver nanoparticles for catalytic applications [13]. Poly(vinyl alcohol) poly(styrene)-poly(ethylene glycol) methacrylate [PVA/PS-PEGMA] composite microgels loaded with silver nanoparticles were synthesized for the same purpose by Lu et al. [17]. Wu et al. investigated gold-poly(N-isopropylacrylamide) [Au-p(NIPAM)] yolk-shell temperature responsive microgels having nanoparticles with tunable selectivity for catalytic reduction of 4-NP and nitrobenzene [15]. Contreras-Cacares et al. prepared gold-poly(N-isopropylacrylamide) [Au-P(NIPAM)] core-shell hybrid system with controllable catalytic activity by changing crosslinking density of microgels [18]. Liu et al. reported catalytic activity of silver-poly(N-isopropylacrylamide) [Ag-P(NIPAM)] hybrid microgels under various conditions of temperature and found that the value of the apparent rate constant (k_{app}) deviates from Arrhenius behavior of temperature dependence of the rate constant [19]. According to best of our knowledge this is the first time that Ag-P(NIPAM-MAA-AAm) hybrid microgels were used as a catalyst for rapid degradation of 4-NP in aqueous medium to evaluate various kinetic parameters.

We synthesized Ag nanoparticles inside multi-responsive P(NIPAM-MAA-AAm) microgels by *in-situ* reduction of silver nitrate ($AgNO_3$) in aqueous medium. Thermal sensitivity and pH responsiveness of

†To whom correspondence should be addressed.
E-mail: m_sidiq12@yahoo.com

microgels were studied by dynamic laser light scattering (DLLS). UV-Visible spectroscopy was used to investigate the pH dependent UV-Visible sensitive property and catalytic behavior of hybrid microgels by measuring the change in absorption spectra of 4-NP as a function of time.

EXPERIMENTAL

1. Materials Used

N-isopropylacrylamide (NIPAM) was recrystallized from a hexane-toluene (1 : 1 volume ratio) mixture and dried in vacuum. Methacrylic acid (MAA) was purified through distillation under reduced pressure. Acrylamide (AAm), N,N-methylenebisacrylamide (BIS), ammonium persulphate (APS), sodium dodecyl sulphate (SDS), silver nitrate ($AgNO_3$), sodium borohydride ($NaBH_4$) and p-nitrophenol (4-NP) were used as received. All the chemicals were purchased from Sigma Aldrich. Deionized water was used throughout the experimental work.

2. Synthesis of P(NIPAM-MAA-AAm) Copolymer Microgels

The microgels were synthesized by free radical emulsion copolymerization of NIPAM, AAm, MAA, and BIS with APS as an initiator [20,21]. The feed composition of microgels is given in Table 1. NIPAM, AAm, MAA, BIS and SDS and 95 mL deionized water were added into a 250 ml three-neck round-bottom flask equipped with a magnetic stirrer, condenser and nitrogen gas (N_2) inlet. The reaction mixture of three-neck round-bottom flask was continuously stirred and heated to 70 °C under continuous N_2 purge. After 30 min, 5 mL of APS (0.05 M) was added into the reaction mixture to initiate the polymerization. The reaction was allowed to proceed for six hours. The prepared P(NIPAM-MAA-AAm) microgels were purified by centrifugation, decantation and washed with water. The resultant microgel was further purified by dialysis of seven days (Spectra/Por molecular porous membrane tubing, cutoff 1,2000-1,4000) against very frequently changed water at room temperature to remove unreacted monomers.

Table 1. Feed composition of P(NIPAM-AA-AAm) microgel particles

NIPAM (mol%)	MAA (mol%)	AAm (mol%)	BIS (mol%)	SDS (g)	APS (.05M)
84	3	8	5	0.05	5 ml

3. *In-situ* Synthesis of Ag Nanoparticles in P(NIPAM-AA-AAm) Copolymer Microgels

Hybrid microgels possessing Ag nanoparticles were synthesized from earlier prepared P(NIPAM-MAA-AAm) microgels. 10 mL of pure microgels was diluted with deionized water up to 50 mL in a 100 mL round bottom flask. 0.2 mL of 0.1 M $AgNO_3$ solution was added into the reaction mixture. This reaction mixture was stirred for one hour at room temperature under continuous N_2 purge. After that, freshly prepared $NaBH_4$ solution (0.02 g in 5 ml water) was added dropwise into the reaction mixture. The reaction mixture was further stirred for two hours at room temperature. Later, the resulting hybrid microgel loaded with Ag nanoparticles was purified by decantation and dialysis of two hours against very frequently changed water.

4. Characterization Techniques

Fourier transform infrared (FTIR) spectroscopy was used to analyze the functional groups present in the microgels. The FTIR spectrum of dried microgels was recorded with Nicole's FTIR Nexus 470 spectrometer. Swelling behavior of microgels was studied by DLLS. DLLS measurements were made by means of commercial

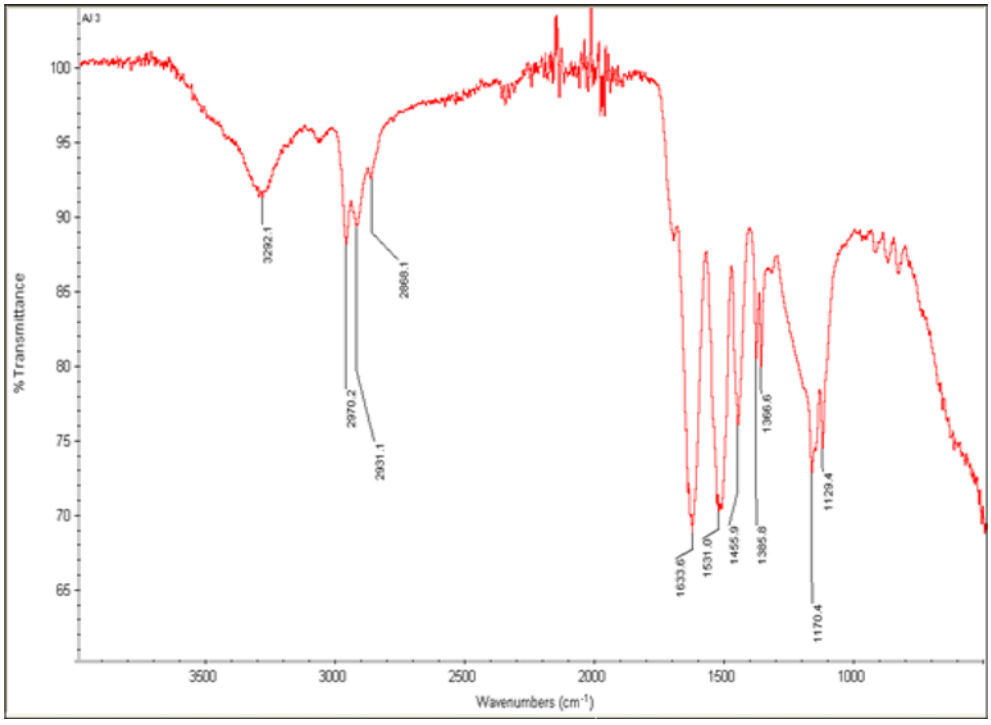

Fig. 1. FTIR spectrum of P(NIPAM-MAA- AAm) microgels.

laser light scattering equipment (Brookhaven) consisting of a BI-200SM motor-driven goniometer and BI-9025AT digital autocorrelator at scattering angle of 90°. A cylindrical 22mWuni-phase Helium-Neon laser (637 nm) with a pinhole of 100 nm and BI-ISTW software was used. A UV-Visible 1601 Shimadzu spectrophotometer with wavelength range of 190-1,100 nm was used to study the optical properties of Ag nanoparticles, effect of pH and temperature on the value of surface Plasmon resonance wavelength (λ_{spr}) of hybrid microgels. Kinetics of catalytic reduction of 4-NP was also studied by using UV-Visible spectrophotometry.

RESULTS AND DISCUSSION

1. Synthesis and FTIR Spectrum of P(NIPAM-MAA-AAm) Microgels

Multiresponsive P(NIPAM-MAA-AAm) microgels were synthesized by free radical precipitation polymerization process. Initiator and monomers react and form crosslinked spheres of microgels. Microgels moieties possess all functional groups as present in monomers as confirmed by FTIR spectrum shown in Fig. 1.

At 70 °C, persulphate ions ($S_2O_8^{2-}$), which are produced from initiator (APS), decompose and produce sulphate radicals ($^{\bullet}SO_4^-$), which initiates the polymerization process [22]. The NIPAM monomer polymerizes and the chain starts to grow; once the chain length reaches a certain critical length it collapses to give precursor particles. The precursor particles then grow by two mechanisms; they either aggregate with other precursor particles or are captured by existing colloidally stable particles. The charge imparted by the initiator stabilizes the microgels. It is necessary to stabilize the precursor particles at early stage of reaction for synthesis of microgel particles. But charge imparted by sulfate radical is not enough for stabilization. Therefore, surfactant is added for further stabilization of microgel particles. After 20 minutes of polymerization process, the color of the solution changed from transparent to milky dispersion, which indicated the formation of microgels. This milky appearance is due to the change in light scattering caused by a change in the dimension of the microgel particles [23]. FTIR spectroscopy was used to identify different functional groups present in the P(NIPAM-MAA-AAm) microgels. Two absorption peaks were observed at 2,970.2 and 2,868.1 cm^{-1} for asymmetric and symmetric stretching of C-H bond, respectively. -C=O, N-H (bending)and C-N (stretching) bonds of amide group shows their characteristic peaks at 1,633.6 cm^{-1}, 1,531.0 cm^{-1} and 1,366.6 cm^{-1}, respectively. Peaks at 1,455.9 and 1,385.8 cm^{-1} appeared for -CH_2- and -CH_3(bending), respectively [24]. FTIR spectrum of microgels shows no peak at 1,655.2 cm^{-1}, which is characteristic for -C=C- double bond present in structure of NIPAM. There are no peaks at 3,032.2 cm^{-1} and 800 cm^{-1} corresponding to =C-H (stretch) of crosslinker and stretching mode of vinyl double bonds, respectively in Fig. 1. Not only the structure of building blocks of microgels but also the presence of water molecules is also confirmed by the FTIR spectrum. The broad and intense peak at 3,292.1 cm^{-1} gives characteristic peak for N-H stretching, showing the presence of hydrogen bonding for water attached to polymer. These results indicate that polymerization has occurred and gel was formed.

2. Temperature Sensitivity of P(NIPAM-MAA-AAm) Microgels at Different pH Values

Temperature sensitivity of P(NIPAM-MAA-AAm) microgel was studied by measuring the hydrodynamic radius (R_h) at different pH values of 2.3, 3.67, 5.43 and 8.2 using DLLS. R_h of microgel particles as a function of temperature at all above pH values is shown in Fig. 2. R_h of prepared microgels increases with increase in pH and decreases by increasing temperature of medium. However, microgels aggregate at very low pH and high temperature as depicted in Fig. 2.

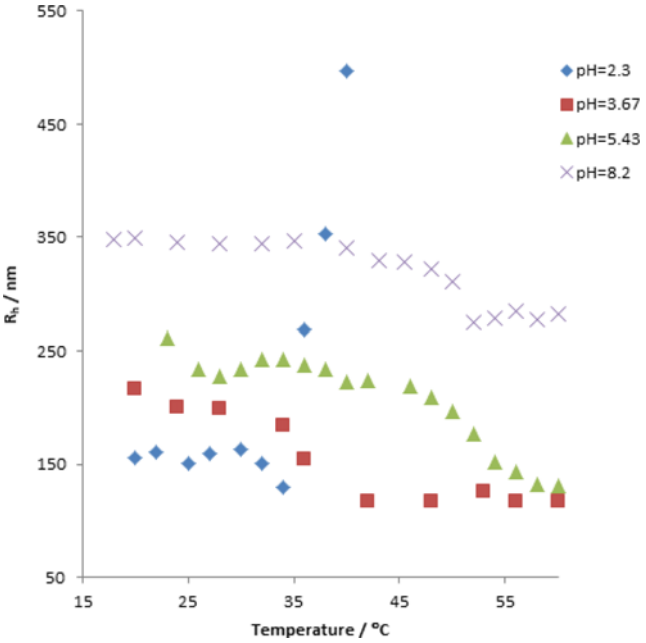

Fig. 2. R_h of P(NIPAM-MAA-AAm) microgels as a function of temperature at different pH values.

Temperature sensitivity of the microgels is significantly pH dependent. At low pH the microgel particle is smaller, but as the pH increases to 3.07, 5.43 and 8.20, the microgel particle increases as manifested by increase in R_h in Fig. 2. R_h at pH 3.07 is less than at pH 5.43, which in turn is less than that of pH 8.20. This is because with the increase in pH, more dissociation of carboxyl groups takes place and charge density increases in microgel network. High negative charge density gives way to greater electrostatic repulsion, and the size of the microgel particles increases [25]. This electrostatic repulsion increases the internal osmotic pressure, which causes the swelling of microgel until the network chains reach upto maximum extension [26]. NIPAM component in the P(NIPAM-MAA-AAm) microgel network undergoes a volume phase transition from swollen to shrunken state by increasing temperature. The driving force for thermally sensitive volume phase transition is a balance between hydrophobic/hydrophilic interactions present between network chains and water molecules [25,26]. Moreover, entropically favored expulsion of water from the polymer matrix along with hydrophobic interactions and hydrogen-bonding between neighboring polymer chains allows the particles to undergo a large volume phase transition with increase in temperature [27,28]. As a result of this phase transition, the state of water molecules in the gel changes from bound water to free water molecules. The transition shifts to slightly higher temperature with increase in pH of medium. Therefore, VPTT at pH 8.20 is greatest among all studied pH conditions. This shift in transition temperature towards higher value is due to increase in number of H-bonds between carboxylate ions and water molecules.

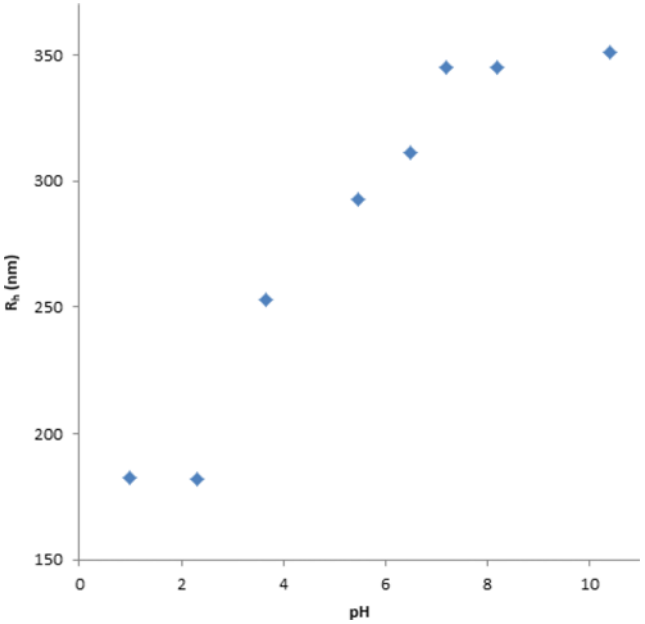

Fig. 3. R_h of P(NIPAM-MAA-AAm) microgels as a function of pH at 25 °C.

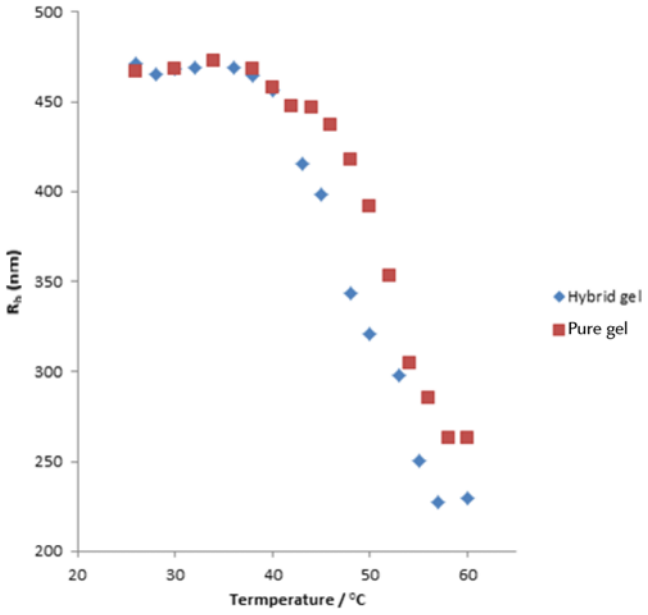

Fig. 4. R_h of pure P(NIPAM-MAA-AAm) microgels and hybrid microgels as a function of temperature at pH=5.43.

At pH 2.3, microgel particles collapse with increase in temperature, but this collapse is followed by aggregation when temperature surpasses ~34 °C. Sudden coagulation of particles is exhibited by abrupt increase in R_h of dispersed particles. This aggregation occurs due to absence of electrostatic repulsion among carboxylic groups in acidic medium and exposure of smaller volume of polymer for bonding with water molecules. This smaller degree of H-bonding and greater hydrophobic interaction of polymer with water molecules causes entrapping of smaller number of water molecules only. Increase in temperature causes breakdown of bonds of polymer with water molecules. Thus, microgel particles shrink with increase in temperature at low pH. Deswollen microgel particles aggregate easily at high temperature in acidic medium, thus causing flocculation [30].

3. pH Sensitivity of P(NIPAM-MAA-AAm) Copolymer Microgels

pH sensitivity of P(NIPAM-MAA-AAm) copolymer microgels was studied as a function of R_h at 25 °C as shown in Fig. 3. MAA groups in the copolymer microgels network cause pH sensitive volume phase transition. Microgel particles show a continuous volume change in three stages with an increase in pH. The size of microgels remains almost constant in the first stage whose pH value range is below the pK_a value of MAA. The second stage is observed when the pH is near to the pK_a value of MAA. In this stage MAA groups start to deprotonate and ionize. This deprotonation produces columbic repulsions among the ionized MAA units, thus increasing the size of the microgel network. At pH value greater than 7.2 all the MAA units are ionized and a maximum swelling is attained. This is the third stage in pH-sensitive volume phase transition [31]. In this way, P(NIPAM-MAA-AAm) microgel draws a sigmoid curve of pH sensitivity.

4. Comparison of Pure and Hybrid Microgels

Swelling behavior of pure and hybrid microgels at pH 5.43 is shown in Fig. 4. It is clear that VPTT of hybrid microgel is shifted to lower value as compared to pure microgel. This decrease in VPTT is due to the incorporation of Ag nanoparticles within voids of microgels. Fabricated Ag nanoparticles occupy space and expel out some water molecules from the interior of the microgel. As a result, the number of H-bonds between polymer chains and water molecules decreases and shifts the VPTT to a relatively lower value. After volume phase transition, the distance between Ag nanoparticles and polymer chains is decreased, which causes complexation of Ag nanoparticles with pendent groups (amide groups) of polymer chains. This complexation increases the degree of shrinking of hybrid microgels. Thus, the presence of Ag nanoparticles used as tool to decrease the VPTT in microgels.

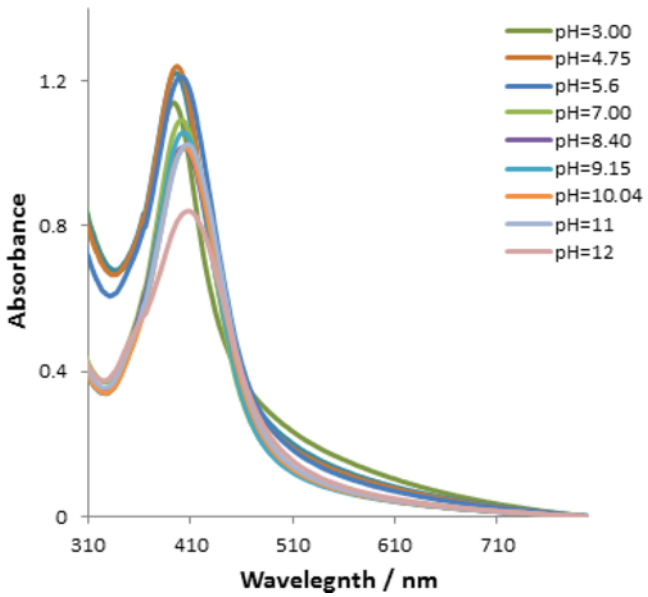

Fig. 5. Ultraviolet-Visible absorption spectra of hybrid microgels at different pH value, at 25 °C.

5. UV-visible Spectroscopic Study of P(NIPAM-MAA-AAm)-Ag Hybrid Microgels

UV-visible spectra of synthesized hybrid microgels was observed by changing the pH of external medium from 3.0 to 12.0 at 25 °C as shown in Fig. 5. A red shift of surface Plasmon resonance band is observed at low temperature with ionization of MAA. This pH-induced red shift is due to merging of particle's surface charge over a small surface area in such a way that the surrounding medium cannot compensate the restoring force effectively, which results in increased electronic oscillations [32,33].

6. Catalytic Activity of Hybrid Microgels

Reduction of 4-NP to 4-AP is chosen as a model reaction to investigate the catalytic activity of synthesized Ag nanoparticles inside the microgels. This reaction is selected due to ease of monitoring and lethal effects of 4-NP on environment. This reaction gives only one product; therefore extent of reaction can be easily followed by measuring absorbance at wavelength 300 and 400 nm with the help of UV-Visible spectrophotometer.

Both 4-NP and catalyst (hybrid gels) absorb at the same wavelength (400 nm). But absorbance measurements of 4-NP during catalytic reduction of 4-NP are not affected by the presence of catalyst due to very low concentration of nanoparticles in the reaction mixture. In our studies, small amounts of catalyst (hybrid microgels) were added in the mixture of 4-NP and $NaBH_4$ aqueous solutions. Reduction was monitored by measuring UV-visible spectra at different time intervals. The height of characteristic peak (λ_{max}) of 4-NP gradually decreased with the passage of time and concomitant appearance of a new peak was observed at ~300 nm as shown in Fig. 6. The gradual decrease in characteristic peak of 4-NP is due to the catalytic effect of Ag nanoparticles. This catalytic effect causes the electron relay from electron donor BH_4^- to acceptor 4-NP by nanoparticles and proceeds the reduction; thus color of the reaction mixture changes from bright yellow to colorless [14,18]. Although the reduction of 4-NP into 4-AP in the presence of aqueous solution of $NaBH_4$ is thermodynamically favorable, the presence of large kinetic barrier due to large potential difference between electron donor and acceptor suppresses the feasibility of this reaction. This large kinetic barrier does not permit the reduction of 4-NP to proceed over time even in large excess of aqueous $NaBH_4$ solution [18,34]. Thus Ag nanoparticles overcome the kinetic barrier and catalyze the reaction [35,36].

A time delay of ~10 min was observed in all cases of catalysis (0.02, 0.04 and 0.06 mL) at room temperature, but it was decreased to ~2 min and reaction was completed in shorter time when temperature was increased to 55 °C, as shown in Fig. 6(a) and 6(b). This time delay is due to the regeneration of Ag nanoparticles by the reduction of oxide layer on their surfaces. Thus, catalyst first gets activated and then starts to catalyze the reaction [37-41].

Pseudo-first-order kinetics with respect to the 4-NP concentration was used for evaluation of k_{app} because concentration of $NaBH_4$ was chosen 100 times greater as compared to that of 4-NP, so rate of these reduction reactions assumed to be independent of the concentration of $NaBH_4$. Thus the kinetic equation is given as follows:

$$\ln\frac{C_t}{C_o} = -k_{app}t \tag{4.1}$$

where, C_t and C_o are the concentrations of 4-NP at time t and 0 min,

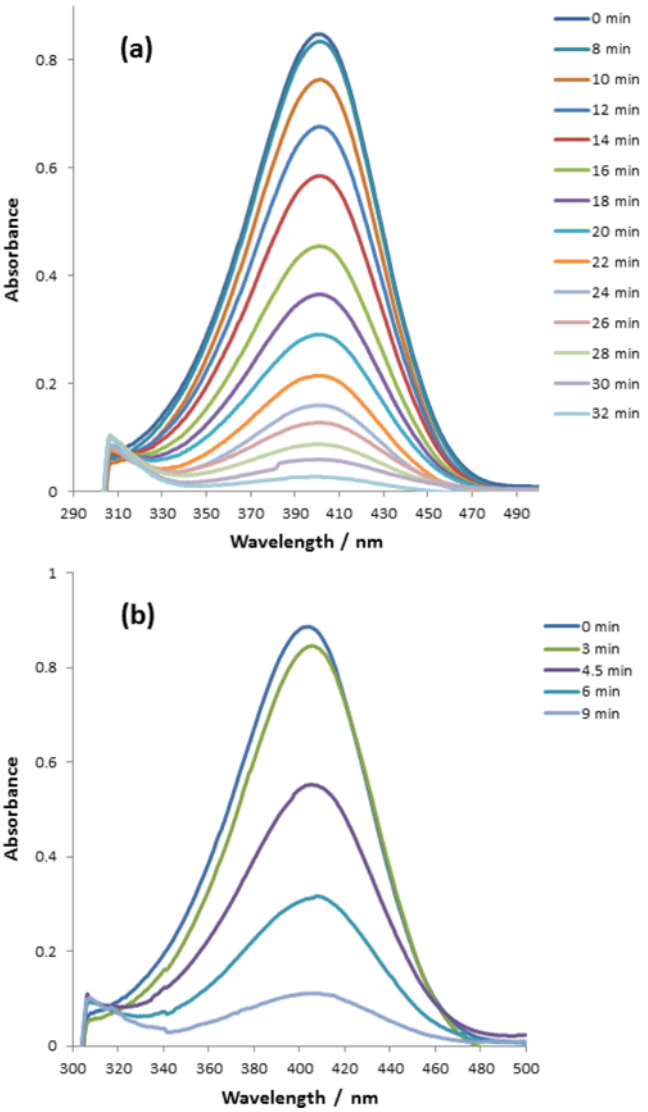

Fig. 6. Plots of absorbance of 4-NP as a function of wavelength in aqueous solution using 0.06 mL of dilute hybrid gel as a catalyst at (a) 25 and (b) 55 °C.

respectively. The concentration ratio C_t/C_o of 4-NP was calculated from the ratio of absorbance of 4-NP at time t (A_t) to that at time 0 min (A_o) because the absorbance of 4-NP is proportional to its concentration in the reaction mixture. k_{app} was calculated from the slope of the straight line portion of the plot of $\ln(C_t/C_o)$ against time. k_{app} increased with the increase in concentration of catalyst at room temperature as well as 55 °C, as observed through Fig. 7(a) and 7(b). This is due to increase in number of available active sites with increment in amount of catalyst. Actually, greater number of active sites increases the effective no. of collisions as a result rate of reaction increases. E_a was calculated by using a modified expression of the Arrhenius equation:

$$\ln\left(\frac{k_1}{k_2}\right) = \frac{E_a}{R}\left[\frac{1}{T_2} - \frac{1}{T_1}\right] \tag{4.2}$$

The values of k_{app} were calculated from the slopes of linear portions of plots and are given in Table 2.

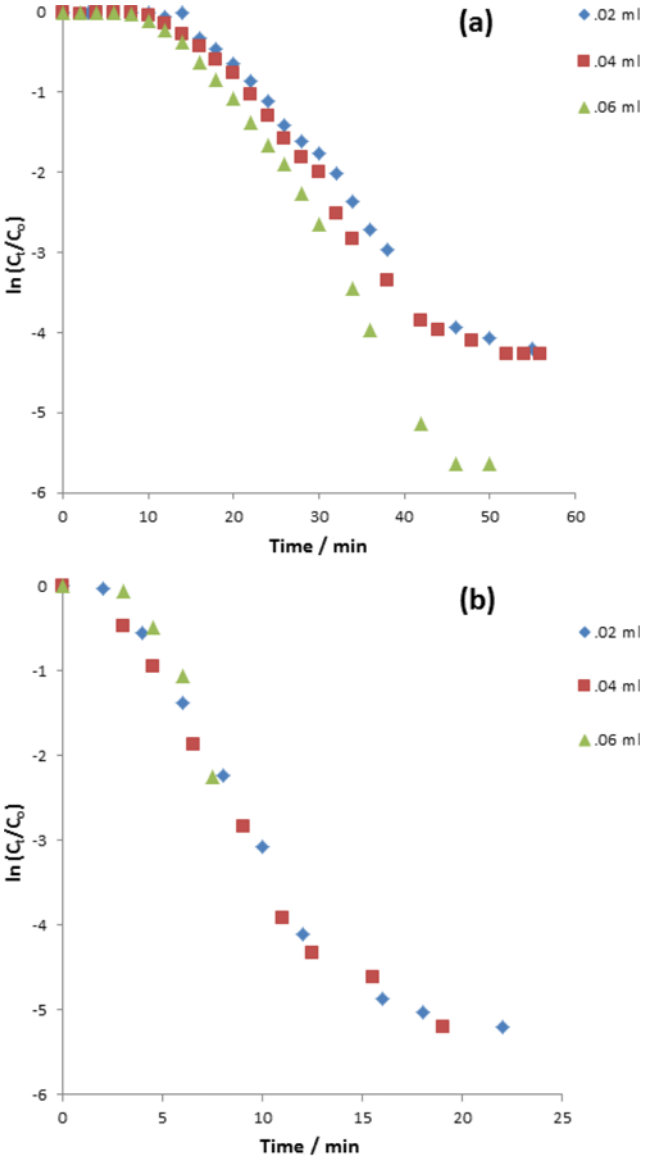

Fig. 7. Effect of concentration of catalyst on k_{app} at temperature (a) 25 and (b) 55 °C.

Table 2. Values of activation energies and apparent rate constants along with the amount of catalyst

Amount of catalyst (mL)	k_{app} at 25 °C (min^{-1})	k_{app} at 55 °C (min^{-1})	E_a (KJ/mol)
0.02	12×10^{-2}	41×10^{-2}	33.28
0.04	15×10^{-2}	43×10^{-2}	28.53
0.06	18×10^{-2}	48×10^{-2}	26.57

7. Comparison with Literature

In our present work, the maximum k_{app} calculated is 48×10^{-2} min^{-1}. This value of k_{app} is larger than reported values in literature for the same catalytic reduction by nanoparticles of the same nature. Previously, Pradhan et al. used Ag nanoparticles to catalyze the reduction of 4-NP to 4-AP using $NaBH_4$ and obtained k_{app} 2.3×10^{-3} sec^{-1} (13.8×10^{-2} min^{-1}) [38]. In 2011, Narayanan and Sakthivel found k_{app} 12.45×10^{-2} min^{-1} using Ag nanoparticle biocomposites as catalyst for the same reaction [42]. Huang et al. studied the catalytic activity of Ag nanoparticles stabilized in amphiphilic star-shaped copolymers and obtained k_{app} equal to 2.84×10^{-2} min^{-1} [16]. Du et al. have reported value of k_{app} 13×10^{-2}, 24×10^{-2}, 37×10^{-2}, 83×10^{-2} min^{-1} by using Ag nanoparticles deposited on Fe_3O_4@SiO_2 for catalytic reduction of 4-NP [14]. Abilash Gangula et al. used biogenic Ag nanoparticles as catalyst for same reduction and found k_{app} 4.06×10^{-3} s^{-1} (24.36×10^{-2} min^{-1}) [11]. It shows that Ag nanoparticles synthesized by our method have higher catalytic activity. This might be due to the relatively smaller size of Ag nanoparticles synthesized inside the microgels; as a result the surface to volume ratio of Ag nanoparticles was increased which in turn increased their catalytic activity. These results also demonstrate that microgels are ideal microreactors for synthesis of metal nanoparticles of smaller and controlled size as well as ideal carrier systems because they prevent aggregation of metal nanoparticles.

CONCLUSIONS

We have accomplished the synthesis and characterization of multi-responsive poly(N-isopropylacrylamide-methacrylic acid-acrylamide) copolymer microgel. Our results showed that low pH and high temperature condition of the external medium results in aggregation of microgels. The synthesized copolymer microgel was successfully employed for the fabrication of sliver nanoparticles. Ultraviolet-visible sensitive properties of silver nanoparticles were studied and a red shift in surface plasmon resonance band was observed with the increase in pH of external medium. So this system has also potential to be used as a pH sensor. The copolymer microgel loaded with silver nanoparticles was found to have excellent catalytic activity, which was studied by monitoring the reduction of p-nitrophenol by an excess of sodium borohydride. Reduction rate was enhanced by increasing the temperature as well as by multiplying the amount of hybrid gel. The maximum apparent rate constant was determined to be 48×10^{-2} min^{-1} at 55 °C. Our results demonstrate that microgel acts as an ideal system for the fabrication of metal nanoparticles and to employ the metal nanoparticles as catalyst.

ACKNOWLEDGEMENTS

We are grateful to Higher Education Commission Pakistan and United States Agency for International Development for financial support under Pak-US Science and Technology Cooperative Program.

REFERENCES

1. T. Vincent and E. Guibal, *Langmuir*, **19**, 8475 (2003).
2. J.-T. Zhang, G. Wei, T. F. Keller, H. Gallagher, C. Stötzel, F. A. Müller, M. Gottschaldt, U. S. Schubert and K. D. Jandt, *Macromol. Mater. Eng.*, **295**, 1049 (2010).
3. M. J. Vaidya, S. M. Kulkarni and R. V. Chaudhari, *Org. Process Res. Dev.*, **7**, 202 (2003).
4. D. E. Bergbreiter, B. L. Case, Y.-S. Liu and J. W. Caraway, *Macromolecules*, **31**, 6053 (1998).
5. C. D. Jones, M. J. Serpe, L. Schroeder and L. A. Lyon, *J. Am. Chem. Soc.*, **125**, 5292 (2003).

6. S. Zhu, C. Du and Y. Fu, *Opt. Mater.*, **31**, 769 (2009).
7. H. Kawaguchi and K. Fujimoto, *Bioseparation*, **7**, 253 (1998).
8. M. Filali, M. A. R. Meier, U. S. Schubert and J.-F. Gohy, *Langmuir*, **21**, 7995 (2005).
9. C.-W. Chen, M.-Q. Chen, T. Serizawa and M. Akashi, *Adv. Mater.*, **10**, 1122 (1998).
10. A. Pich, A. Karak, Y. Lu, A. K. Ghoshf and H.-J. P. Adler, *Macromol. Rapid Commun.*, **27**, 344 (2006).
11. A. Gangula, R. Podila, M. Ramakrishna, L. Karanam, C. Janardhana and A. M. Rao, *Langmuir*, **27**, 15268 (2011).
12. J. Zhang, S. Xu and E. Kumacheva, *J. Am. Chem. Soc.*, **126**, 7908 (2004).
13. S. Wunder, F. Polzer, Y. Lu, Y. Mei and M. Ballauff, *J. Phys. Chem. C*, **114**, 8814 (2010).
14. X. Du, J. He, J. Zhu, L. Sun and S. An, *Appl. Surf. Sci.*, **258**, 2717 (2012).
15. S. Wu, J. Dzubiella, J. Kaiser, M. Drechsler, X. Guo, M. Ballauff and Y. Lu, *Angew. Chem. Int. Ed.*, **51**, 2229 (2012).
16. X. Huang, Y. Xiao, W. Zhang and M. Lang, *Appl. Surf. Sci.*, **258**, 2655 (2012).
17. Y. Lu, P. Spyra, Y. Mei, M. Ballauff and A. Pich, *Macromol. Chem. Phys.*, **208**, 254 (2007).
18. R. Contreras-Cáceres, A. Sánchez-Iglesias, M. Karg, I. Pastoriza-Santos, J. Pérez-Juste, J. Pacifico, T. Hellweg, A. Fernández-Barbero and L. M. Liz-Marzán, *Adv. Mater.*, **20**, 1666 (2008).
19. Y.-Y. Liu, X.-Y. Liu, J.-M. Yang, D.-L. Lin, X. Chen and L.-S. Zha, *Colloids Surf., A*, **393**, 105 (2012).
20. Z. H. Farooqi, A. Khan and M. Siddiq, *Polym. Int.*, **60**, 1481 (2011).
21. W. Wu, T. Zhou and S. Zhou, *Chem. Mater.*, **21**, 2851 (2009).
22. J.-T. Zhang, C.-J. Pan, T. Keller, R. Bhat, M. Gottschaldt, U. S. Schubert and K. D. Jandt, *Macromol. Mater. Eng.*, **294**, 396 (2009).
23. J.-T. Zhang, X.-L. Liu, A. Fahr and K. Jandt, *Colloid. Polym. Sci.*, **286**, 1209 (2008).
24. C. Wang, N. T. Flynn and R. Langer, *Adv. Mater.*, **16**, 1074 (2004).
25. S. Zhou and B. Chu, *J. Phys. Chem. B*, **102**, 1364 (1998).
26. Z. H. Farooqi, W. Wu, S. Zhou and M. Siddiq, *Macromol. Chem. Phys.*, **212,** 1510 (2011).
27. M. Shibayama, S.-y. Mizutani and S. Nomura, *Macromolecules*, **29**, 2019 (1996).
28. M. Seno, M. Lin and K. Iwamoto, *Colloid. Polym. Sci.*, **269**, 873 (1991).
29. H. Naeem, Z. H. Farooqi, L. A. Shah and M. Siddiq, *J. Polym. Res.* DOI:10.1007/s10965-012-9950-1.
30. K. Kratz, T. Hellweg and W. Eimer, *Colloids Surf., A*, **170**, 137 (2000).
31. W. Wu, T. Zhou, A. Berliner, P. Banerjee and S. Zhou, *Chem. Mater.*, **22**, 1966 (2010).
32. S. Underwood and P. Mulvaney, *Langmuir*, **10**, 3427 (1994).
33. B. J. Wiley, S. H. Im, Z.-Y. Li, J. McLellan, A. Siekkinen and Y. Xia, *J. Phys. Chem. B*, **110**, 15666 (2006).
34. S. Jana, S. K. Ghosh, S. Nath, S. Pande, S. Praharaj, S. Panigrahi, S. Basu, T. Endo and T. Pal, *Appl. Catal. A*, **313**, 41 (2006).
35. Y. Deng, Y. Cai, Z. Sun, J. Liu, C. Liu, J. Wei, W. Li, C. Liu, Y. Wang and D. Zhao, *J. Am. Chem. Soc.*, **132**, 8466 (2010).
36. Y. Zhu, J. Shen, K. Zhou, C. Chen, X. Yang and C. Li, *J. Phys. Chem. C*, **115**, 1614 (2010).
37. S. Panigrahi, S. Basu, S. Praharaj, S. Pande, S. Jana, A. Pal, S. K. Ghosh and T. Pal, *J. Phys. Chem. C*, **111**, 4596 (2007).
38. N. Pradhan, A. Pal and T. Pal, *Colloids Surf., A*, **196**, 247 (2002).
39. Y. Lu, Y. Mei, M. Ballauff and M. Drechsler, *J. Phys. Chem. B*, **110**, 3930 (2006).
40. S. Praharaj, S. Nath, S. K. Ghosh, S. Kundu and T. Pal, *Langmuir*, **20**, 9889 (2004).
41. Y. Mei, G. Sharma, Y. Lu, M. Ballauff, M. Drechsler, T. Irrgang and R. Kempe, *Langmuir*, **21**, 12229 (2005).
42. K. B. Narayanan and N. Sakthivel, *J. Hazard. Mater.*, **189**, 519 (2011).